2021 20th IEEE Intersociety Conference on Thermal and Thermomechanical Phenomena in Electronic Systems (iTherm) | 978-1-7281-8539-2/21/$31.00 ©2021 IEEE | DOI: 10.1109/ITherm51669.2021.9503214

Heat Spreading and Heat Removal Needs of a Novel Power Electronics Package with Integrated Cooling

Ahmet Mete Muslu
George W. Woodruff School of Mechanical Engineering
Georgia Institute of Technology
Atlanta, GA 30332
metemuslu@gatech.edu

Ryan Wong
School of Materials Science and Engineering
Georgia Institute of Technology
Atlanta, GA 30332
rnt.wong@gatech.edu

Vanessa Smet
George W. Woodruff School of Mechanical Engineering
Georgia Institute of Technology
Atlanta, GA 30332
vanessa.smet@prc.gatech.edu

Yogendra Joshi
George W. Woodruff School of Mechanical Engineering
Georgia Institute of Technology
Atlanta, GA 30332
yogendra.joshi@me.gatech.edu

ABSTRACT

Power electronics modules increasingly require compact and high-performance thermal packaging solutions capable of handling the resulting higher power densities. Double-sided cooled packages have been a promising solution to significantly reduce overall thermal resistance of packages below 0.2 K.cm^2/W. However, components with only single function prevent further reduction in the overall volume of the package. In this paper, a novel integrated cooling strategy is introduced for further miniaturization of power electronics package, where copper leads or vapor chambers are utilized as multi-functional layers for both power delivery and heat spreading. Parametric thermo-mechanical modeling is carried out with heat conduction-based models to understand the heat spreading and heat removal behavior of the integrated cooling solution. Despite the reduced number of package layers in the integrated cooling solution, thermomechanical performance enhancement is demonstrated over the standard package when vapor chambers are used to spread heat more effectively. Relative variation of one-dimensional and spreading thermal resistances of vapor chambers shows that an increase in the overall thickness of vapor chambers is only useful up to a certain cut-off thickness, beyond which thermal performance is reduced and package volume is increased excessively. If sufficiently high effective lateral thermal conductivity is achieved, use of ultra-thin vapor chambers is found to be even more advantageous to maximize power density of future power modules.

KEY WORDS: Power electronics, silicon carbide (SiC), vapor chamber.

NOMENCLATURE

ICS	Integrated cooling solution
VC	Vapor chamber
VSI	Voltage Source Inverter
SVPWM	Space Vector Pulse Width Modulation
MOSFET	Metal-oxide-semiconductor Field-effect Transistor
HTC	Heat transfer coefficient (W/m^2.K)
R	Thermal resistance
P	Power loss (W)
T	Temperature (K)
$\overline{T}$	Average temperature (K)
k	Thermal conductivity (W/m.K)
t	Thickness (m)

Subscripts

s	Spreading
l	Lateral
th	Thermal
ev	Evaporator side
con	Condenser side
1D	One-dimensional

Authorized licensed use limited to: Georgia Institute of Technology. Downloaded on August 18,2021 at 04:48:55 UTC from IEEE Xplore. Restrictions apply.

I. INTRODUCTION

Emerging power electronics must be designed to meet ever-increasing power density requirements. Transition from Si to SiC-based devices in applications such as electrified transportation requires the adoption of effective thermal management solutions to maintain reliable operating temperatures. Conventional power modules with a large number of package layers increase the overall size and cost of the system. Reliability of these modules is seriously threatened by increased thermal resistances and induced hot spots. Failure modes associated with contact stress, substrate cracking, and wire bond breakage are commonly observed in standard packages [1], [2], [3].

To reduce device-to-coolant thermal resistance of a package, materials with higher thermal conductivity may be incorporated, or some layers in the package may be eliminated. Removal of layers may allow for increased power density of the module as long as effective cooling strategies are adopted. To reduce thermal resistance of packages, many recent power module packages include a thick lead frame structure made of copper as a bottom substrate, which spreads heat, and eliminates a number of package layers. Double sided cooling has been recently adopted to further reduce package thermal resistance [4], [5], [6]. Specific thermal resistance was reduced from 0.3-0.4 K.cm^2/W in single side cooled standard packages to below 0.2 K.cm^2/W in double side cooled modern packages [7].

To further improve thermal performance of power packages, combination of the baseplate and heat sink to remove the TIM layer [8] and cooling the ceramic substrate directly [9] have been investigated. Cooling can be brought even closer by eliminating the Direct Bonded Copper (DBC) layer and directly cooling the power devices. Boteler et al [10] replaced single-function components by multifunctional components and removed heat directly from devices using a dielectric fluid. A dielectric cooling concept via jet impingement on finned surfaces, where the electrical interconnects were cooled to obtain improved performance over conventional DBC based designs was also explored [11].

Advanced cooling solutions with porous media, micro fins, jet impingement, and microchannels, where single or two-phase cooling can be used for all these alternative solutions were explored. Chein et al. [12] demonstrated that utilizing copper foams as a heat sink material improved thermal performance compared to single-channel, plate-fin, and pin fin heat sinks due to flow characteristics and the high heat transfer area. Ndao et al. [13] achieved enhancement factors up to 3.03 or around 200% rise in the heat transfer coefficients using an array of micro pins with diameters of 125 µm, heights of 230 µm, and pitches of 250 µm on the jet impingement surface. Lee et al. [14] investigated a micro cooler's thermal performance with multiple microchannels (10 µm × 90 µm) created on a SiC substrate to employ impingement cooling using methanol as a working fluid. They predicted the required heat transfer coefficients to remove heat fluxes above 30 kW/cm^2 at the device level for various flow conditions. Adoption of these high heat flux cooling solutions is critical, as more compact packaging techniques such as 3D chip stacking are developed to maximize power density, while minimizing parasitic inductance [15].

Thermal management solutions must be compact, cost-effective, simple to manufacture, and highly reliable. Their integration with modern packages should be able to remove and spread heat effectively in a minimum package volume to maximize the power density. Thus, significant care should be given for solutions that focus on eliminating additional layers in the packaging, where hot spots may arise if spreading of heat is insufficient. This problem becomes even more serious as the number of devices in close proximity within a single package increases within the reduced footprint area of the package. Indirect liquid cooling techniques, that integrate a cooler with the power devices, must provide effective heat spreading within highly compact form factors. Direct immersion cooling solutions provide an effective alternative for heat spreading and heat removal. However, use of dielectric fluids with low thermal conductivity, and concerns regarding leakage and material compatibility have resulted in their slower adoption [16].

The effective heat spreading, and heat rejection capabilities of the thermal management solution are critical to finding new solutions for high power electronics. As a promising candidate, phase-change cooling approaches such as pool boiling, and condensation have been explored intensively in recent studies due to its capability to handle higher heat fluxes [17], [18]. However, several concerns including reduced cooling efficiency due to non-condensable gases and stability problems are raised to adopt these solutions reliably. In this paper, a novel packaging module with integrated cooling solution using electrical terminals as heat spreaders is studied for emerging power electronics. DBC layers used in the standard packages are eliminated. The heat spreading, and heat removal capabilities of the approach are investigated.

II. METHODOLOGY

The standard power packaging module with integrated cooling configurations examined in this study is shown in Fig. 1. Three different configurations have been studied to assess thermomechanical performance of the integrated cooling solution:

- Configuration 1: Standard power card with copper lead frames/heat spreaders
- Configuration 2: Integrated cooling solution with copper lead frames/heat spreaders
- Configuration 3: Integrated cooling solution with vapor chambers used as lead frames/heat spreaders

Steady state conduction-based computational models were created in ANSYS Workbench for these three different configurations. It should be noted that DBC and thermal interface material (TIM) layers were removed for the

Authorized licensed use limited to: Georgia Institute of Technology. Downloaded on August 18,2021 at 04:48:55 UTC from IEEE Xplore. Restrictions apply.

configuration with integrated cooling. Instead, copper lead frames and vapor chambers were utilized to function both as heat spreaders and electrical terminals. For each configuration, corresponding to a half-bridge structure, four SiC devices were utilized based on the power loss calculations summarized in Table IV and Table V.

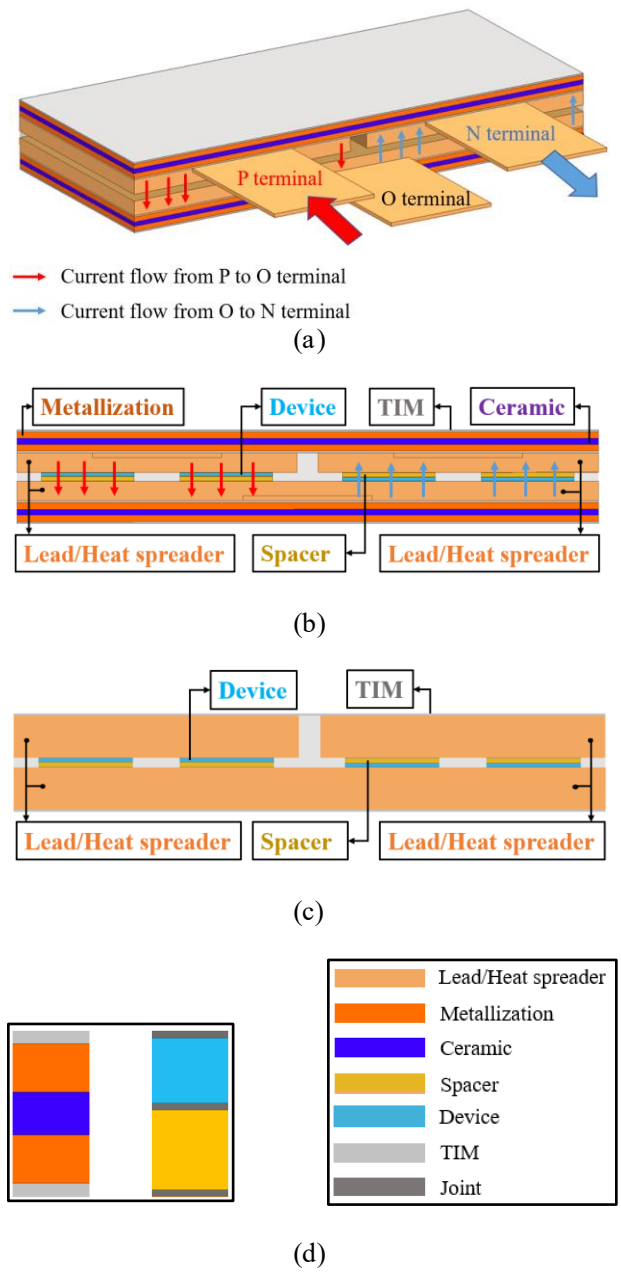

Fig. 1. (a) 3D view of standard power card (b) Cross-sectional view of standard power card (c) Package with integrated cooling solution (d) Close-up view of package layers

For each configuration, the package footprint and thicknesses of layers, other than the lead frame/heat spreader layer, have been kept fixed during the analysis. The baseline dimensions of the standard package were determined based on a Mixed-Variable Bayesian Optimization approach as described in [19]. Then, thickness of heat spreading layers, effective thermal conductivity of vapor chambers, and heat generation rates of devices have been varied in different parts of the study. For computational efficiency, heat transfer coefficients were defined at the top and bottom surfaces of the packages, which were exposed to ambient temperature of 40 ºC. The defined heat transfer coefficient was decided based on a computational study providing minimum required HTCs corresponding to maximum allowed junction temperature (the highest temperature in devices) of 175°C at different heat flux conditions (see Section III and Fig.3).

Dimensions and material properties of different components of the package configurations are listed in Table I and Table II. Before conducting thermal and mechanical simulations, power loss calculations were made to determine total losses in the package. Dimensions, thermal conductivity, and mechanical properties of the SiC devices utilized in this study are given in Table I, Table II, and Table III respectively. In addition, maximum driving current of those devices is specified as 160 A. Using the device specifications provided by STMicroelectronics [20] and specifications of a 50 kW Voltage Source Inverter with Space Vector Pulse Width Modulation (SVPWM) (given in Table IV), total power losses in the package have been calculated based on the guidelines given in [21].

As shown in Table IV, based on the battery voltage of 400 V, for the targeted output power of 50 kW, the output current through the inverter is calculated as 208 A, which is higher than the maximum rating of 160 A for the device. Therefore, two devices are necessary per switch position, with equal sharing of current between them. For two positions with two devices, in total four devices are needed for the targeted output power described above.

TABLE I. DIMENSIONS OF THE PACKAGE COMPONENTS

Components	Dimensions (mm × mm × mm)
Upper leads (heat spreader)	15.4 × 13.9 × t (varied)
Lower lead (heat spreader)	32 × 13.9 × t (varied)
Metallization	32 × 13.9 × 0.34
Ceramic	32 × 13.9 × 0.3
Spacer	5.1 × 5.1 × 0.22
Device	5.1 × 5.1 × 0.18
TIM	32 × 13.9 × 0.1
Joint	5.1 × 5.1 × 0.02
Mold	32 × 13.9 × 1.46

Authorized licensed use limited to: Georgia Institute of Technology. Downloaded on August 18,2021 at 04:48:55 UTC from IEEE Xplore. Restrictions apply.

TABLE II. THERMAL CONDUCTIVITIES OF PACKAGING MATERIALS

Components	Materials	Thermal Conductivity (W/m.K)
Upper and lower leads (heat spreaders)	Cu	400
	Vapor chamber	*k_z = 300 *k_x = k_y = varied: (900, 1200, 1500, 5500)
Metallization	Cu	400
Ceramic	AlN	160
Spacer	Cu	400
Device	SiC	Temperature-dependent 385.5 (at 40ºC)
TIM	Parker T670	3
Joint	Sintered silver	250

*k_x and k_y are in-plane thermal conductivities in the lateral direction, while k_z is through-plane effective thermal conductivity in the vertical direction.

TABLE III. MATERIALS AND MECHANICAL PROPERTIES OF THE PACKAGE COMPONENTS

Materials	Isotropic Elasticity		Coefficient of Thermal Expansion (10^{-6}/ºC)
	Young's Modulus (GPa)	Poisson's Ratio	
SiC	411	0.16	4
Cu and Vapor chamber	117	0.34	16
AlN	325	0.25	5
TIM (Parker T670)	1.6	0.3	150
Sintered silver	72	0.37	20

TABLE IV. SPECIFICATIONS OF INVERTER

Battery Voltage (V)	400
Line to Line Voltage (V)	230.9
Phase Voltage (V)	133.3
Output Power (kW)	50
Switching Frequency (kHz)	20
Fundamental Frequency (kHz)	60
Power Factor	0.85
Modulation Index	1
Output RMS Current (A)	147.1
Output Peak Current (A)	208.8

Conduction and switching losses for the power package have been determined for the peak driving current of 208.8 A, as summarized in Table V. Total power losses were then calculated as the sum of conduction and switching losses generated in a MOSFET and Diode, which are placed in one SiC device. Considering the total power losses generated in a device (92.9 W) and dimensions of the SiC device (5.1 mm × 5.1 mm), heat flux of 357 W/cm^2 were defined for each device in the package as an input parameter in thermal models. Thermal and mechanical models were also coupled to determine the corresponding mechanical stress in devices due to different coefficient of thermal expansion (CTE) of layers. Linear elastic models were utilized in the analysis. Although non-linear models such as Anand's model are expected to give more accurate results, mechanical simulations with elastic models are useful for relative comparison of the performance in different configurations in a time efficient manner.

TABLE V. LOSSES FOR ACTIVE DEVICES

Conduction Loss ($P_{C, MOSFET}$)	39.4 W
Switching Loss ($P_{SW, MOSFET}$)	33.7 W
Conduction Loss ($P_{C, DIODE}$)	19.2 W
Switching Loss ($P_{SW, DIODE}$)	0.65 W
Total Losses (per device)	92.9 W
Total Losses (four devices)	**371.8 W**
Efficiency	97.8%

Computational models were built for three different configurations by including the package components in Fig. 1 at dimensions given in Table I, with material properties given in Table II and Table III. A mesh independence study was carried out to reduce the computational time and sensitivity of the results to the number of mesh elements for the standard package and package with the integrated cooling solution (ICS). Considering the parametric analyses in the study, mesh study was performed for the geometry with the lowest thickness of heat spreading layer (0.45 mm) to provide sufficient number of mesh elements for all parametric models. Based on the convergence of results (maximum variation of 0.1°C), optimum mesh element size was determined as 0.4 mm for the standard package and 0.20 mm for the package with the integrated cooling solution (ICS). This corresponds to around 210,000 elements for the standard package and 35,000 elements for the package with ICS (see Fig. 2).

In addition, steady state thermal and mechanical models were coupled to extract Von Mises stresses in devices due to the thermal loads in the structure. Computationally efficient comparison of thermomechanical performance was aimed among different configurations. Therefore, linear material models were utilized instead of non-linear models. Under this limitation, the optimum mesh element size which was

Authorized licensed use limited to: Georgia Institute of Technology. Downloaded on August 18,2021 at 04:48:55 UTC from IEEE Xplore. Restrictions apply.

determined for the thermal models was also utilized in thermomechanical models.

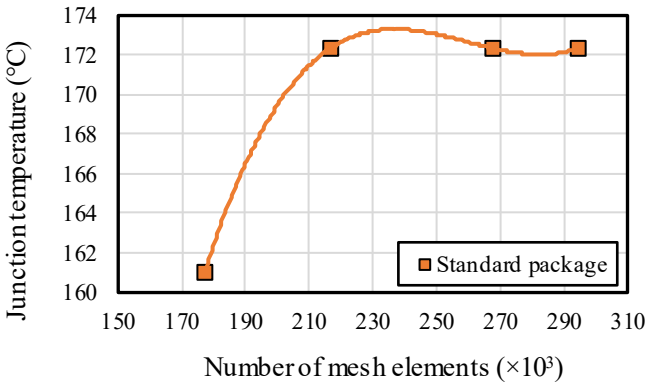

(a)

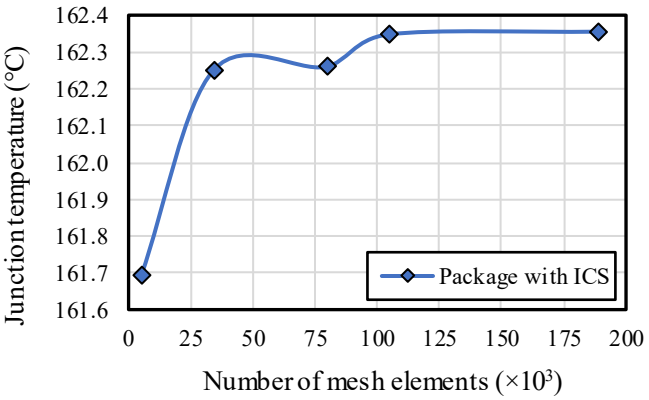

(b)

Fig. 2. Mesh independence study (a) for the standard package, and (b) package with the integrated cooling solution (ICS)

III. RESULTS AND DISCUSSIONS

In this section, thermomechanical performance of the proposed integrated cooling solution was compared with the standard package. First, the minimum heat transfer coefficients required to keep the junction temperature of the package below 175°C were identified to avoid oversizing of the cooling structures, and maximize the power density of the package. Analysis was conducted numerically with the standard package having 1 mm thickness of copper leads or heat spreaders, operating at heat flux in the range of 100 W/cm^2 to 1,000 W/cm^2. The minimum required heat transfer coefficients obtained for the standard package are given in Fig. 3. Based on this analysis, a heat transfer coefficient of 5,000 W/m^2.K was chosen for the operation at 357 W/cm^2 in order to provide sufficient cooling and keep the volume of cooling structures small enough.

In transition from the standard power card to the integrated cooling solution, thickness of heat spreader is found to be as an important design parameter. In fact, increasing thickness of heat spreading layer indefinitely is not a good approach for optimal performance, since it would increase the overall size of the system and reduce power density. As the thickness of the heat spreading layer is increased, spreading thermal resistance is expected to drop, while the conduction thermal resistance rises. Therefore, trade-offs between these two different thermal resistances determine thermal behavior of power packages as heat spreader thickness is changed.

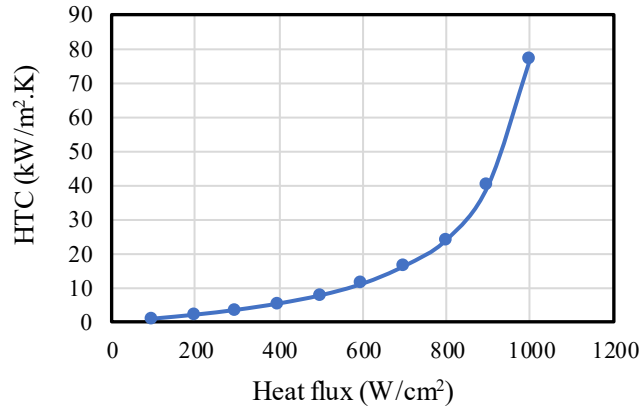

Fig. 3. Minimum required heat transfer coefficients to keep junction temperature below 175 °C at each heat flux condition

The impact of thickness of the heat spreading layer on junction temperature is examined in Fig. 4 at an imposed heat flux of 357 W/cm^2. The integrated cooling solution was represented by various configurations, including copper leads, and vapor chambers with different lateral effective thermal conductivities. It is observed that junction temperature in the package is significantly lowered when additional layers are removed, and the cooling is brought closer to the devices. Therefore, integrated cooling solution with reduced number of layers is found to be promising since it significantly decreases junction temperature of a standard package by 10°C to 15°C depending on the heat spreader thickness. It should be noted, however, that heat spreading thickness should be increased enough to maximize the thermal performance improvement in the case of integrated cooling solution with copper leads. Initially, junction temperature decreases dramatically as thickness of heat spreading layer is increased in the lower thickness range (0.45 mm to 1 mm). However, increasing the heat spreading layer thickness beyond a certain cut-off thickness value only raises the package volume without improving thermal performance. In order to increase power density of a package, it is important to provide sufficient heat spreading and heat removal without increasing the volume significantly. Then, the question arises if it is possible to maximize the thermal performance at lower heat spreading layer thicknesses. With this objective, copper heat spreaders were replaced by vapor chambers at different lateral thermal conductivities. As shown in Fig. 4, the integrated cooling configuration consisting of vapor chambers with lateral thermal conductivity above 900 W/m.K outperforms the standard power card, and integrated cooling with copper heat spreaders at any thickness value in the range of 0.45 mm to 4 mm. For the cases with k_l = 900 W/m.K and k_l = 1,500 W/m.K, junction temperature continues to

Authorized licensed use limited to: Georgia Institute of Technology. Downloaded on August 18,2021 at 04:48:55 UTC from IEEE Xplore. Restrictions apply.

decrease until the cut-off thickness value is reached, then junction temperature starts to rise again. In fact, this behavior is attributed to the relative variation of spreading and 1D thermal resistances of vapor chambers as their thicknesses are increased.

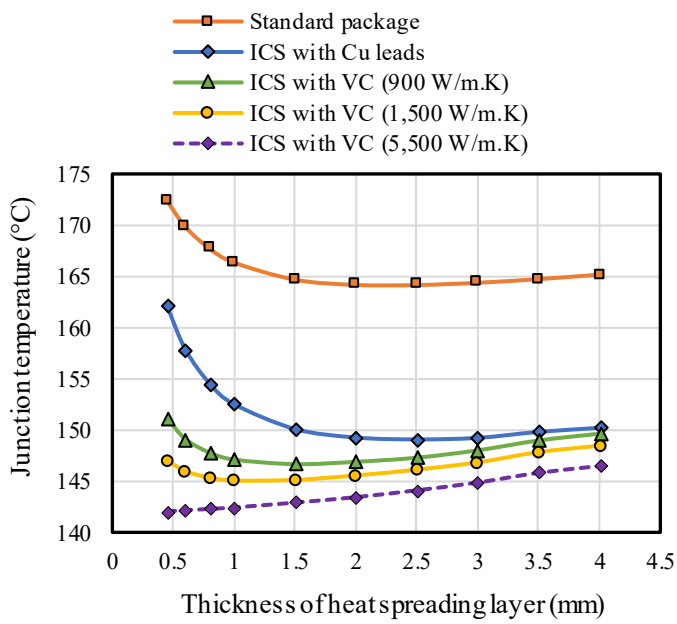

Fig. 4. Variation of junction temperature with thickness of heat spreading layer for different package configurations

To better understand the thermal behavior of vapor chambers and its impact on the package performance, the total thermal resistance of vapor chambers was formulated below as the sum of one-dimensional (1D) and spreading thermal resistances of vapor chamber [22]:

$$R_{VC} = R_{VC,1D} + R_{VC,s} \tag{1}$$

where

$$R_{VC} = \frac{T_{ev} - \bar{T}_{con}}{\dot{Q}} \tag{2}$$

$$R_{VC,1D} = \frac{\bar{T}_{ev} - \bar{T}_{con}}{\dot{Q}} \tag{3}$$

$$R_{VC,s} = \frac{T_{ev} - \bar{T}_{ev}}{\dot{Q}} \tag{4}$$

where T_{ev} and $\bar{T}_{ev}$ represent maximum and average temperature at the evaporator side of the vapor chamber, while $\bar{T}_{con}$ stands for the average temperature at the condenser side of the vapor chamber.

Relative variation of one-dimensional (1D), spreading and total thermal resistances of vapor chamber at the lower side was analyzed in Fig. 5 with respect to heat spreading layer thickness for effective lateral thermal conductivities of k_l = 900 W/m.K, and k_l = 5,500 W/m.K respectively. For the vapor chamber with k_l = 900 W/m.K, spreading thermal resistance of vapor chamber decreases as its thickness is increased. However, after a certain cut-off thickness value, total thermal resistance of vapor chamber reaches a saturation point. After this point, it increases slightly due to the increase in 1D thermal resistance of the vapor chamber with thickness. In the case of vapor chamber with k_l = 5,500 W/m.K, the relative variation in 1D thermal resistance is even more dramatic, compared to the change in spreading thermal resistance. Thus, total thermal resistance of the vapor chamber keeps increasing with thickness. This behavior is also reflected in the junction temperature response in Fig. 4 for the integrated cooling solution with k_l = 5,500 W/m.K.

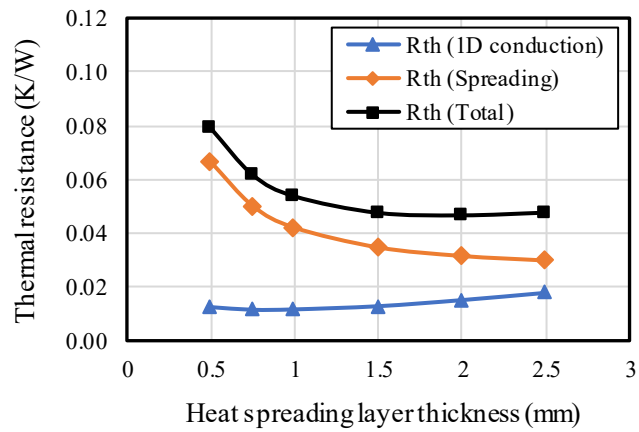

(a)

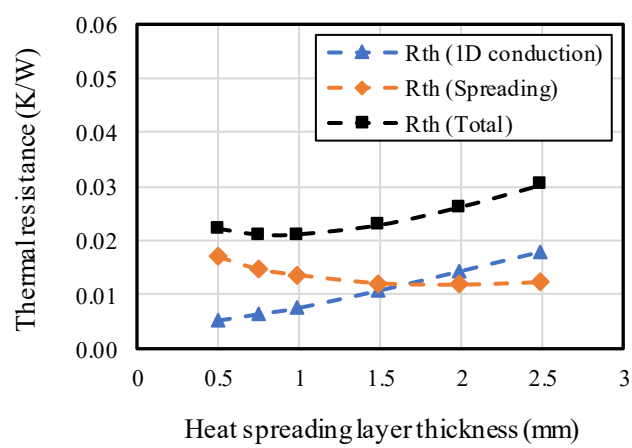

(b)

Fig. 5. Relative variation of thermal resistances of vapor chamber with heat spreading layer thickness (a) for k_l = 900 W/m.K, and (b) for k_l = 5,500 W/m.K

As a result, it is concluded that cut-off thickness value is shifted to the left, as effective thermal conductivity increases. With sufficiently high effective lateral thermal conductivity, the increase in 1D thermal resistance dominates over the decrease

Authorized licensed use limited to: Georgia Institute of Technology. Downloaded on August 18,2021 at 04:48:55 UTC from IEEE Xplore. Restrictions apply.

in spreading resistance, as thickness of layer is increased. Thus, ultra-thin vapor chambers become more advantageous when a sufficiently high lateral thermal conductivity value is achieved. This would both improve heat spreading, and reduce the overall package thickness.

As previously discussed, it is important to reduce minimum required heat transfer coefficients to minimize the size of cooling structure and package volume at a certain operation condition. Therefore, it is useful to analyze if the integrated cooling solution with vapor chambers is able to reduce the minimum required HTCs at ultra-high heat flux conditions. Fig. 6 shows the reduction of HTCs compared to the standard package of the same thickness (1 mm) to keep maximum device temperature below 175ºC. Lateral effective thermal conductivity of 900 W/m.K was chosen for the comparison, considering in-plane effective thermal conductivities reported in literature and future improvements in vapor chamber technology [23].

It is observed that at each heat flux condition integrated cooling solution is able to maintain junction temperature of 175ºC with lower HTCs. This shows that the required cooling volume can be reduced with the proposed solution as the number of package layers is reduced at the same time. In fact, use of ultra-thin vapor chambers plays an even greater role in reducing minimum required HTCs at higher heat flux conditions. This is illustrated in the figure with a greater reduction in the required HTCs from 28.2% to 79.7% as the heat flux is increased from 500 W/cm^2 to 1,000 W/cm^2.

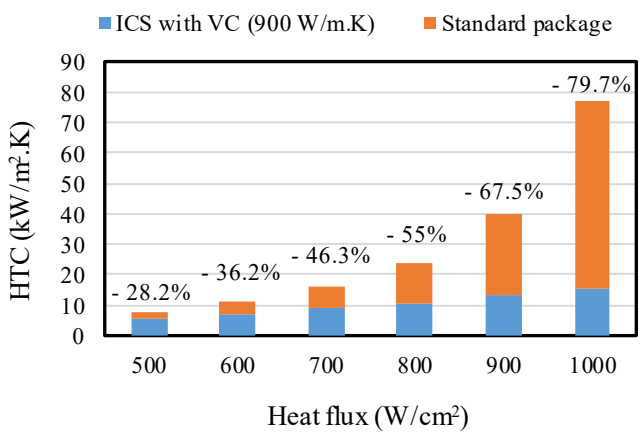

Fig. 6. Reduction in minimum required heat transfer coefficients in transition from standard power card to integrated cooling solution with vapor chambers

Junction temperature behavior for different configurations is analyzed for the same heat spreader thickness (1 mm) at different heat flux conditions in Fig. 7.

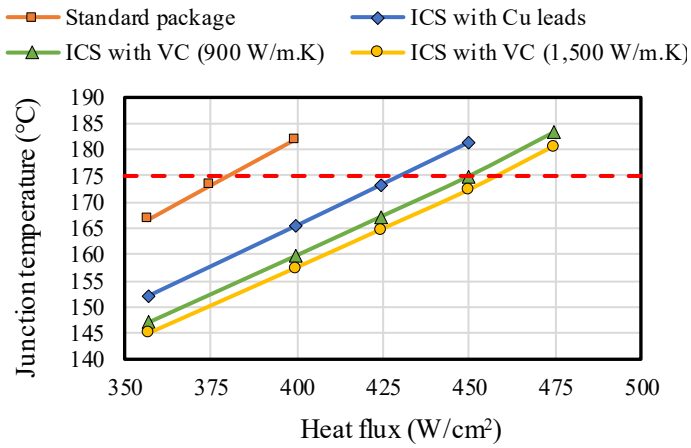

Fig. 7. Junction temperature behavior of various configurations of the package at different heat flux conditions

It is noticed that removing the additional layers from the standard package, and directly cooling over the heat spreaders results in a decrease in junction temperature. In addition, replacing copper heat spreaders with vapor chambers both reduces volume of the package, and also decreases junction temperature, as shown in the figure. Maximum power that can be handled with the integrated cooling solution was also investigated in the analysis for the maximum allowable temperature of 175°C. While the maximum heat flux that can be handled is 375 W/cm^2 for the standard package, it is elevated to 425 W/cm^2 for the integrated cooling with copper heat spreaders and to 450 W/cm^2 for the integrated cooling solution with vapor chambers. As is noticed, the integration of vapor chamber did not significantly increase the maximum power amount that can be handled, but it was more effective in reducing temperature gradients as presented in the following analyses.

Temperature uniformity in a single device and among different devices in the package is also important in providing similar operating conditions, and ensuring reliability of devices over long-term operation [24]. Therefore, a comparison of temperature profiles was made to observe the temperature uniformity of devices with respect to their positions. Temperature profile over the top surface of the lower heat spreader was created with a line extending from one side of the package to another, as shown in Fig. 8.

Authorized licensed use limited to: Georgia Institute of Technology. Downloaded on August 18,2021 at 04:48:55 UTC from IEEE Xplore. Restrictions apply.

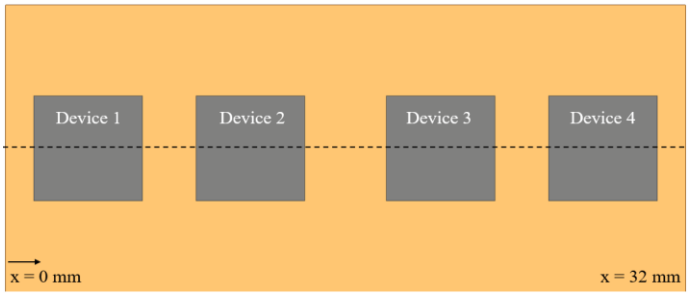

(a)

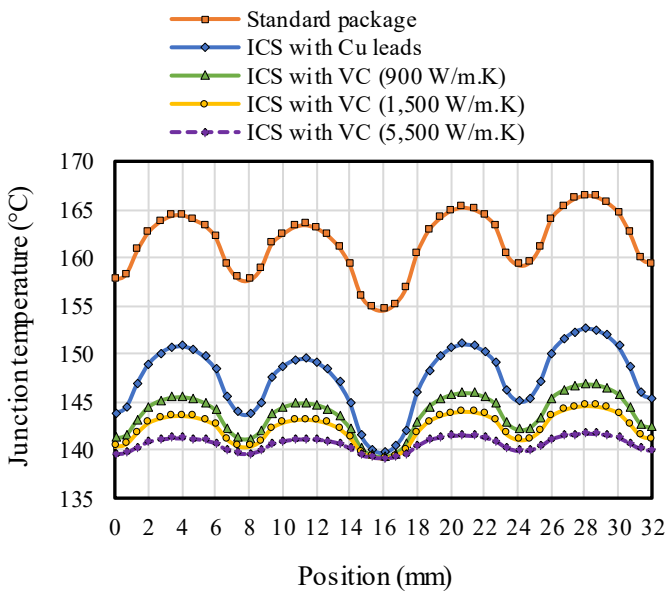

(b)

Fig. 8. (a) Temperature profile line extending from one side of the vapor chamber surface to another (b) Temperature profile of the package for different configurations of the package

As shown in the figure, standard package and integrated cooling solution with copper spreaders leads to relatively high ΔT in devices. However, when those copper heat spreaders are replaced by vapor chambers in the integrated cooling solution, the temperature profile is smoothened, as lateral effective thermal conductivity of a vapor chamber is increased. The impact of increased heat spreading can be seen more clearly in Fig. 9 for different cases including standard package, integrated cooling solution with copper heat spreaders, and integrated cooling solution with vapor chambers (k_l = 900 W/m.K). Thus, replacing copper heat spreaders with vapor chamber not only reduces junction temperature but also decreases the temperature variation in devices.

Since junction temperature and temperature variation in devices affect the reliability of the devices [24], maximum von Mises (equivalent) stresses induced on the devices were extracted in Fig. 10. Due to the large area contacts with different coefficient of thermal expansion of layers, standard power card yielded the highest stress compared to the integrated cooling solutions.

With increased heat spreading, integrated cooling with vapor chambers was found to be the most advantageous in terms of minimizing the stress in devices as the effective thermal conductivity increases.

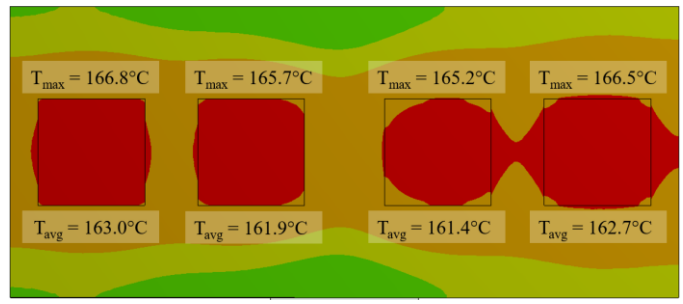

(a)

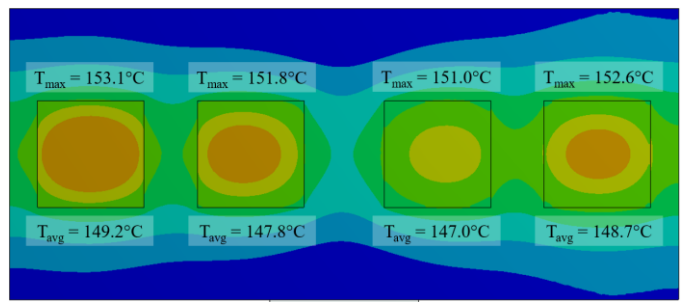

(b)

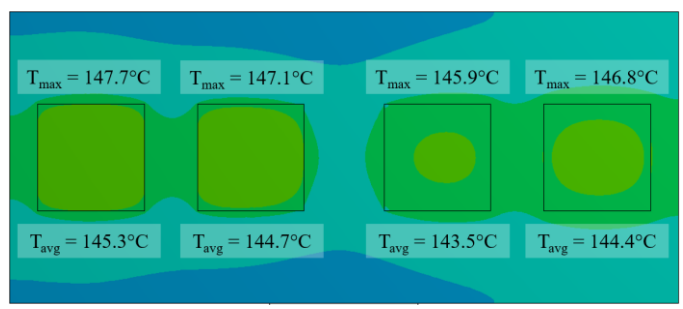

(c)

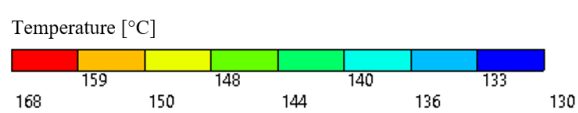

Fig. 9. Temperature distribution and heat spreading effect in (a) Standard package, (b) Integrated cooling solution with Cu leads, and (c) Integrated cooling solution with vapor chambers (k_l = 900 W/m.K)

Authorized licensed use limited to: Georgia Institute of Technology. Downloaded on August 18,2021 at 04:48:55 UTC from IEEE Xplore. Restrictions apply.

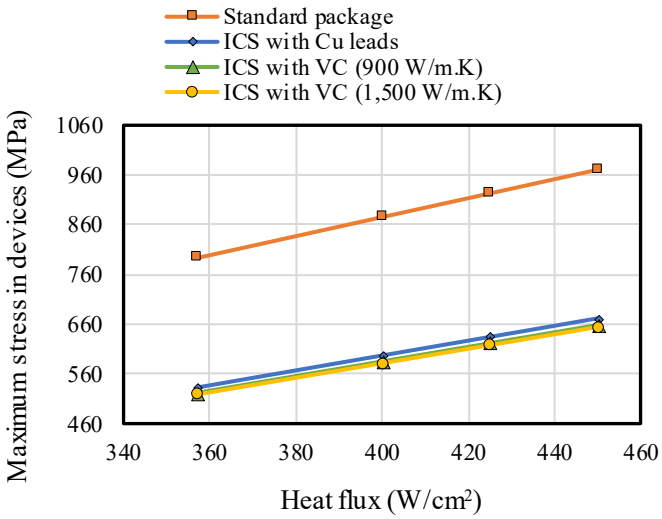

Fig. 10. Variation of maximum stress in devices at different heat flux conditions

IV. SUMMARY AND CONCLUSIONS

In this study, integrated cooling approach with copper leads and vapor chambers was introduced, and thermomechanical performance of various configurations was analyzed. Analysis was conducted for a given footprint area (32 mm x 13.9 mm) and layer thicknesses of a power package. Based on the power loss calculations, parts of analyses were conducted for a heat flux condition of 356 W/cm^2, while the others were carried out by examining the performance at various heat flux conditions to obtain the maximum power handling capability of the package and observe the performance of integrated cooling solution at ultra-high heat flux conditions.

Based on the analyses, the following conclusions were reached to consider in the future packaging solutions:

- As thickness of heat spreader increases, junction temperature of the package is reduced up to a cut-off value, and then it increases due to the relative variation of spreading and 1D thermal resistances of vapor chamber.
- As lateral effective thermal conductivity of the vapor chamber is increased, cut-off thickness value is reduced.
- At a sufficiently high lateral thermal conductivity of vapor chambers, increase of layer thickness raises junction temperature of a package with integrated cooling solution. Therefore, use of ultra-thin vapor chambers with the lowest possible thickness is more advantageous if sufficiently high lateral thermal conductivity is achieved.
- Integrated cooling with vapor chambers is even more effective at higher heat flux conditions in terms of reducing overall cooling size of the package and maximizing power density.
- Although the use of vapor chambers did not increase the maximum power handling capability significantly, it was quite effective in reducing temperature gradients and maximum stresses in devices.

As a result, bringing cooling closer to the devices with the integrated cooling solution by using the copper leads as heat spreaders and electrical terminals is a promising approach to improve thermal performance and power density of the standard packages. Furthermore, replacing the copper leads with vapor chambers further improves the performance of a package by reducing temperature gradients, maximum stress in devices and the overall volume.

With the analysis and conclusions drawn in this study, future studies will focus on multi-physics performance of the integrated cooling solution, considering the electrical performance of the package as well.

ACKNOWLEDGMENT

This work was supported by the Industry Consortium at the Georgia Tech Packaging Research Center (PRC). The authors would like to thank the member companies of the industry consortium at the 3-D Systems Packaging Research Center and the Bosch team including Dr. Michael Guyenot, Dr. Martin Rittner, Dr. Alexander Frank, and Dr. Marco Lenz for their support.

REFERENCES

[1] H. Ye, M. Lin, and C. Basaran, "Failure Modes and FEM Analysis of Power Electronic Packaging", Finite Elements in Analysis & Design, Vol. 38 No. 7, pp. 601-612, 2002.

[2] M. Ciappa and P. Malberti, "Plastic-strain of Aluminium Interconnections during Pulsed Operation of IGBT Multichip Modules", Quality and Reliability Engineering International, vol. 12, no. 4, pp. 297–303, 1996.

[3] C. Durand, M. Klingler, D. Coutellier, and H. Naceur, "Power Cycling Reliability of Power Module: A survey", IEEE Transactions on Device and Materials Reliability, vol. 16, no. 1, pp. 80–97, 2016.

[4] T.A. Burress, C.L. Coomer, S.L. Campbell, A.A. Wereszczak, J.P. Cunningham, L.D. Marlino, L.E. Seiber, and H.T. Lin, "Evaluation of the 2008 Lexus LS 600H Hybrid Synergy Drive System." Oak Ridge National Laboratory (ORNL), TN, 2009.

[5] Z. Liang, "Integrated Double Sided Cooling Packaging of Planar SiC Power Modules", IEEE Energy Conversion Congress and Exposition (ECCE), pp. 4907- 4912, Montreal, Canada, September 20-24, 2015.

[6] Z. Liang, "Planar-bond-all: A Technology for Three-dimensional Integration of Multiple Packaging Functions into Advanced Power Modules", in

Authorized licensed use limited to: Georgia Institute of Technology. Downloaded on August 18,2021 at 04:48:55 UTC from IEEE Xplore. Restrictions apply.

Integrated Power Packaging (IWIPP), 2015 IEEE International Workshop on. IEEE, 2015, pp. 115–118.

[7] H. Lee, V. Smet, and R. Tummala, "A Review of SiC Power Module Packaging Technologies: Challenges, Advances, and Emerging Issues", IEEE Journal of Emerging and Selected Topics in Power Electronics, 1–1, 2019.

[8] K. Bennion, J. Cousineau, J. Lustbader, and S. Narumanchi, "Novel Power Electronics Three-dimensional Heat Exchanger", 14th Intersociety Conference on Thermal and Thermomechanical Phenomena in Electronic Systems (ITherm), pp. 1055-1063. Orlando, FL, May 27-30, 2014.

[9] T.A. Burress, S.L. Campbell, C.L. Coomer, C.W. Ayers, A.A. Wereszczak, J.P. Cunningham, L.D. Marlino, L.E. Seiber, and H.T. Lin, "Evaluation of the 2010 Toyota Prius Hybrid Synergy Drive System." Oak Ridge, TN. 2011.

[10] L.M. Boteler, V. A. Niemann, D. P. Urciuoli, and S.M. Miner, "Stacked Power Module with Integrated Thermal Management", 2017 IEEE International Workshop On Integrated Power Packaging (IWIPP), April 2017.

[11] G. Moreno, "Power Electronics Thermal Management", National Renewable Energy Laboratory (NREL), DOE Vehicle Technologies Office, 2019 Annual Merit Review and Peer Evaluation Meeting.

[12] R. Chein, H. Yang, T.H. Tsai, and C. Lu, "Experimental Study of Heat Sink Performance using Copper Foams Fabricated by Electroforming", Microsystem Technologies, Vol. 16 No. 7, 2010, pp. 1157-1164.

[13] S. Ndao, H.J. Lee, Y. Peles, and M.K. Jensen, "Heat Transfer Enhancement from Micro Pin Fins subjected to An Impinging Jet", International Journal of Heat and Mass Transfer, Vol. 55 No. 1-3, 2012, pp. 413-421.

[14] H. Lee, D.D. Agonafer, Y. Won, F. Houshmand, C. Gorle, M. Asheghi, and K.E. Goodson, "Thermal Modeling of Extreme Heat Flux Microchannel Coolers for GaN-on-SiC Semiconductor Devices", Journal of Electronic Packaging, Vol. 138 No. 1, 2016, pp. 010907.

[15] C. Yao, Z. Wang, W. Li, H. Li, J. Qian, C. Han, F. Luo, and J. Wang, "Comparison Study of Common-mode Noise and Thermal Performance for Lateral Wire-bonded and Vertically Integrated High Power Diode Modules", IEEE Transactions on Power Electronics, vol. 33, no. 12, pp. 10 572–10 582, 2018.

[16] J. Broughton, V. Smet, R.R. Tummala, and Y.K. Joshi, "Review of Thermal Packaging Technologies for Automotive Power Electronics for Traction Purposes", Journal of Electronic Packaging, 140(4), 040801, 2018.

[17] C.A. Sayed, O. Ghaffari. F. Grenier, W. Tong, M.Bolduc, J. Morissette, S. Jasmin, J. Sylvestre, "Localized pool boiling and condensation experiments over functional CPU: Optimizing the overall thermal resistance via different heat transfer scenarios", 2020 19th IEEE Intersociety Conference on Thermal and Thermomechanical Phenomena in Electronic Systems (ITherm), Orlando, FL, USA, 2020, pp. 410-416.

[18] O. Ghaffari, F. Grenier, J. Morissette, M. Bolduc, S.Jasmin, J. Sylvestre, "Pool boiling experiment of dielectric liquids and numerical study for cooling a microprocessor", 2019 18th IEEE Intersociety Conference on Thermal and Thermomechanical Phenomena in Electronic Systems (ITherm), Las Vegas, NV, USA, 2019, pp. 540-545.

[19] H.M.Torun, "Machine Learning based Design and Optimization for High-Performance Semiconductor Packaging and Systems", Doctoral thesis, Georgia Institute of Technology, 2020-11-23.

[20] Online source: www.st.com.

[21] H. Muhsen, S. Hiller, and J. Lutz, "Three-phase voltage source inverter using SiC MOSFETs — Design and Optimization," in 2015 17th European Conference on Power Electronics and Applications (EPE'15 ECCE-Europe), 8-10 Sept. 2015, pp. 1-9.

[22] Y.-S. Chen, K.-H. Chien, T.-C. Hung , C.-C. Wang, Y.-M. Ferng, and B.-S. Pei, "Numerical Simulation of a Heat Sink Embedded with a Vapor Chamber and Calculation of Effective Thermal Conductivity of a Vapor Chamber", Applied Thermal Engineering, 29(13), 2655–2664, 2009.

[23] A. Bar-Cohen, K. Matin, N. Jankowski, and D. Sharar, "Two-Phase Thermal Ground Planes: Technology Development and Parametric Results" Journal of Electronic Packaging, 137(1), 010801, 2014.

[24] V. Smet, "Aging and failure modes of IGBT power modules undergoing power cycling in high temperature environments", Doctoral thesis in Electrical, Electronics, Photonics and Systems Engineering, Information, Structures, Systems (Montpellier; Doctoral School; 2009-2014), 25-11-2010.

Authorized licensed use limited to: Georgia Institute of Technology. Downloaded on August 18,2021 at 04:48:55 UTC from IEEE Xplore. Restrictions apply.